Mammalian-Membrane-Two-Hybrid (MaMTH): a novel split-ubiquitin assay for investigation of signaling pathways in human cells

Julia Petschnigg[1], Bella Groisman[1], Max Kotlyar[2], Mikko Taipale[3], Yong Zheng[4], Christoph F. Kurat[1,12], Azin Sayad[1], J. Rafael Sierra[2], Mojca Mattiazzi Usaj[1], Jamie Snider[1], Alex Nachman[1], Irina Krykbaeva[3], Ming-Sound Tsao[2,5,6], Jason Moffat[1,7], Tony Pawson[4,13], Susan Lindquist[3,8,9], Igor Jurisica[2,5,10], and Igor Stagljar[1,7,11*]

[1]Donnelly Centre, University of Toronto, Ontario, Canada

[2]Princess Margaret Cancer Centre, University Health Network, University of Toronto, Ontario, Canada

[3]Whitehead Institute for Biomedical Research, Cambridge, USA

[4]Samuel Lunenfeld Research Institute, Mount Sinai Hospital, Toronto, Ontario, Canada

[5]Department of Medical Biophysics, University of Toronto, Ontario, Canada

[6]Department of Laboratory Medicine and Pathobiology, University of Toronto, Ontario, Canada

[7]Department of Molecular Genetics, University of Toronto, Ontario, Canada

[8]Howard Hughes Medical Institute, Cambridge, USA

[9]Department of Biology, Massachusetts Institute of Technology, Cambridge, USA

[10]Department of Computer Science, University of Toronto, Ontario, Canada

[11]Department of Biochemistry, University of Toronto, Ontario, Canada

[12]Current address: Cancer Research UK London Research Institute (LRI), Clare Hall Laboratories, South Mimms, Hertfordshire, UK

[13]deceased

*Corresponding Author:

Igor Stagljar

Phone: 1-416-946-7828

Fax: 1-416-978-8287

E-mail: igor.stagljar@utoronto.ca

Abstract

Cell signaling, one of the key processes involved in human health and disease, is coordinated by numerous membrane protein-protein interactions (PPIs) that change in response to stimuli. Currently, there is a lack of assays that can detect these changes in stimuli- and disease-related contexts. Here, we present a novel split-ubiquitin-method for the detection of integral membrane PPIs in human cells, termed Mammalian-Membrane-Two-Hybrid (MaMTH). We highlight the strength of this technology by showing that it detects stimuli (hormone/agonist)- and phosphorylation-dependent PPIs. Importantly, it can detect changes in PPIs conferred by mutations such as those in oncogenic ErbB-receptor variants or by treatment with drugs like the tyrosine-kinase inhibitor erlotinib. Using MaMTH as a screening assay, we identified CRKII as an interactor of oncogenic EGFR-L858R, promoting persistent activation of aberrant signaling. In conclusion, our study illustrates that MaMTH is a powerful tool for investigating dynamic interactomes of human integral membrane proteins.

Introduction

Membrane proteins, comprising nearly 30% of the proteome[1], play pivotal roles in cellular processes and are major targets for the development of new therapeutics. Understanding membrane protein function depends on their physical interactions within protein complexes. However, it is a major challenge to investigate the complex protein network associated with the malfunction of integral membrane proteins leading to various diseases.

Cancerous signaling pathways are often triggered by variations in phosphorylation patterns of signaling components leading to increased association with down-stream adaptors and subsequently, to malignant cell proliferation. Thus, mammalian assays that can identify changes in PPIs conferred by aberrant signaling pathways help us to understand disease mechanisms and define novel drug targets. One of the most extensively studied signaling networks involves the ErbB family of receptor tyrosine kinases. ErbB signaling is implicated in cancer progression and has been well analyzed by classical biochemical methods[2, 3]. However, mass-spectrometry-based biochemical assays are labour-intensive and often unsuitable for detecting transient and modification-dependent PPIs. A range of mammalian methods have emerged to uncover PPIs as a function of physiological context[4]. Genetic systems like protein-fragment-complementation assays (PCAs) are powerful methods to investigate context-dependent PPIs and have been successfully applied to map membrane PPIs[4-7]. PCAs and variants have been applied to detect ligand-dependent interactions of ErbB family receptors and ligand-induced GPCR-activation[8, 9] as well as hormone-induced ErbB heterodimerization[10]. Techniques like FRET/BRET[11] or MAPPIT[4] are valuable tools to study signaling pathways, but are technically challenging or not suitable for mapping PPIs of integral membrane proteins. Despite the availability of these methods, there remains a lack of cell-based high-throughput assays that can sensitively detect changes in interaction patterns in response to drugs, natural stimuli or ligands.

Here, we present a novel split-ubiquitin two-hybrid approach, called the Mammalian-Membrane-Two-Hybrid (MaMTH) that addresses the challenge of studying PPIs of full-length integral membrane proteins in stimuli-dependent contexts. We demonstrate that MaMTH can detect the phosphorylation state of oncogenic ErbB receptors through measurement of phosphorylation-dependent protein recruitment. Moreover, we show for the first time that MaMTH can monitor erlotinib-inhibited interactions of oncogenic EGFR receptors in a dose-dependent manner. Using MaMTH in a targeted screen to map interaction changes between wildtype and oncogenic EGFR, we identified CRKII as a major driver of oncogenic signaling. In conclusion, we present MaMTH as a highly sensitive and powerful new genetic assay for use in the study of dynamic changes in the PPI patterns of integral membrane proteins.

Results

Development of MaMTH

MaMTH is based on the split-ubiquitin assay[12] and is derived from its variant, the membrane yeast two-hybrid (MYTH)[13-15]. A membrane bait protein is tagged with the C-terminal half of ubiquitin (Cub) and a chimeric transcription factor (TF), and a cytosolic or membrane-bound prey is tagged with the N-terminal half of ubiquitin (Nub). Upon bait and prey interaction, the split-halves form pseudo-ubiquitin, which is recognized by cytosolic deubiquitinating enzymes (DUBs), resulting in TF-cleavage and reporter gene expression (**Fig. 1a**). Substantial protein engineering was performed to transfer the original yeast MYTH to mammalian cells. First, we tested suitable TFs[16-18] for reporter gene activation in 8xlexAops-luciferase and 5xGAL4UAS-luciferase stable HEK293T cells and found that TFs GAL4(1-147)-mNFkB(364-550) and mLexA(1-202)-VP16(413-490) resulted in highest luciferase induction (**Supplementary Fig. 1a**). Next, we tested various linkers[7, 13, 19] between cDNAs and Cub/Nub and found that glycine-serine linkers allowed for the most efficient ubiquitin reconstitution (**Supplementary Fig. 1b**). We also tested a range of Nub variants and determined that human Wt-NubI and Cub displayed the best affinity, differing from the yeast system which requires the use of mutant 'NubG' with reduced Cub affinity[12, 20] (**Supplementary Fig. 1c**). Finally, we incorporated LexA mutant (mLexA[21]), lacking an NLS-like sequence, into bait constructs, reducing background activation (**Supplementary Fig. 1d**). **Supplementary Fig. 1e** shows the final arrangement of all constructs.

MaMTH performance and validation

5xGAL4UAS-luciferase/GFP or 8xlexAops-luciferase/GFP HEK293T reporter cells stably expressing ErbB4-Cub-TF were infected with Nub-Shc1 or Nub-Grb2 preys (positive controls) or Nub-Fabp5 (negative control) and the activation of GFP and luciferase reporters was measured (**Fig. 1b** and **Supplementary Fig. 2**). MaMTH detected PPIs between ErbB4-Cub-TF and positive controls in all TF-set-ups tested. Reporter gene activation correlated with transcription factor cleavage, as monitored by Western blot. In general, both GFP and luciferase reporters can be used in MaMTH, but since the luciferase set-up is faster and more easily scaled up, further experiments were performed using luciferase reporters.

Localization of ErbB-Cub-GFP-TF fusions demonstrated that tagging does not affect proper plasma membrane localization (**Supplementary Fig. 3a**). To ensure that NubI does not lead to nonspecific interactions, we reconstituted known PPIs, and observed comparable results for all bait proteins tested (**Fig. 1c** and **Supplementary Fig. 3b-f**). Known interactors of EGFR and ErbB4 such as Grb2, Shc1 and Hsp90 were detected well above negative prey controls (**Fig. 1c** and **Supplementary Fig. 3d**). Cfl1 and GAPDH, previously shown to interact with EGFR[22], also interacted with ErbB4-bait in

our assay. We also successfully reconstituted other known interactions, such as the heterodimerization of the GPCRs GABBR1 and GABBR2 (**Supplementary Fig. 3e-f**). Both co-transfection and infection of bait/prey showed comparable results (**Supplementary Fig. 4**).

MaMTH allows detection of context-dependent interactions

Monitoring agonist-induced interaction between β2-AR and β-arrestin

Next, we reconstituted the PPI between human β2-adrenergic receptor (β2-AR) and β-arrestin. β-arrestin associates with β2-AR once an agonist such as isoproterenol binds the receptor, leading to G-protein signaling and GRK-induced phosphorylation[23]. MaMTH readily detected agonist-dependent β2-AR and β-arrestin interaction (**Fig. 2a**). To test if this interaction is specific, we mutated GRK phosphorylation sites on β2-AR-Cub-mLexA-VP16. Mutant β2-AR-baits were expressed at similar levels and properly localized (**Fig. 2b-c** and **Supplementary Fig. 5**). Mutating GRK6- or GRK2-phosphorylation sites on the receptor led to decreased β-arrestin binding upon agonist treatment, whereas a combination of GRK6 and GRK2 mutations abolished agonist-induced β-arrestin-binding (**Fig. 2c**). Binding of β2-AR-GRK6/GRK2-Cub-mLexA-VP16 mutant to mutant Nub- β-arrestin-R169E, which can bind non-phosphorylated β2-AR[24], was comparable to β2-AR-Wt (**Fig. 2d**). Notably in this case, TF cleavage did not directly correlate with luciferase activity, however due to the nature of the reporter system, even small differences in levels of free TF can lead to detectable differences in luciferase expression. Cells expressing unrelated interaction pairs were unaffected by agonist treatment (**Supplementary Fig. 6a**), excluding nonspecific agonist effects.

MaMTH allows mapping of specific phospho-tyrosines involved in PPIs

ErbB family members contain 89 tyrosine-residues on their cytosolic terminus[3], some of which are involved in stimuli-dependent interactions with adaptor proteins such as Grb2. We used MaMTH to map phosphorylation-sites on ErbB receptors responsible for Grb2 binding, confirming the previously reported binding sites on EGFR[3], and monitoring an additive decrease in Nub-Grb2-binding upon introduction of single (EGFR-Y1092A) and double mutations (EGFR-Y1092A/Y1138A), whereas Nub-GAPDH binding was unaffected (**Fig. 3a).** Another SH2-domain-containing prey protein, Nub-CRKII, also showed a binding pattern similar to that of Nub-Grb2. Furthermore, ErbB2-Y1139A- and ErbB3-Y1262A/Y1199A-Cub-GAL4-NFkB baits harboring mutations in known Grb2 phospho-tyrosine binding sites showed significantly reduced binding to Nub-Grb2 upon ligand-binding compared to wildtype (**Fig. 3b**). Interestingly, consistent with the study by Schulze *et al.*[3], no effect on Nub-Shc1 binding was observed in the Grb2-phospho-site mutant ErbB2-Y1139A-Cub-GAL4-NFkB, but an effect could still be detected in ErbB3-Y1262A/Y1199A-Cub-GAL4-NFkB bait (**Fig. 3b**).

Monitoring phosphorylation-dependent interactions

RTK signaling cascades are mediated by numerous phosphorylation-dependent PPIs[25]. MaMTH could detect stimuli-dependent PPIs in cells co-expressing ErbB2-Cub-GAL4-mNFkB and Nub-Grb2, Nub-Shc1 or Nub-Hsp90, showing increased luciferase activity compared to starvation conditions (**Supplementary Fig. 7a**), indicative of activated ErbB2. This was even more pronounced when cells were transfected directly in starvation media (**Supplementary Fig. 7b**). Residual luciferase activity in serum-starved cells reflects basal receptor activity. Next, we showed that treatment with a non-specific tyrosine kinase inhibitor (TKI-PD158780) reduced phosphorylation of ErbB4, resulting in lower Nub-Shc1-binding (**Supplementary Fig. 7c**).

We then used MaMTH to monitor the phosphorylation state of oncogenic ErbBs displaying constitutively active kinase activity. Oncogenic ErbB4 mutations[26] were introduced into ErbB4-Cub-GAL4-NFkB baits and tested for Nub-Shc1 binding (**Fig. 4a**). We detected a significant increase in Nub-Shc1 recruitment in ErbB4-E542K- and ErbB4-E872K-Cub-GAL4-NFkB baits (but not ErbB4-R544W) compared to wildtype in the absence of serum, correlating with their oncogenic nature. Moreover, two oncogenic variants, EGFR-G719S- and EGFR-L858R-Cub-GAL4-NFkB[27], resulted in increased Nub-Shc1 binding in serum-independent conditions (**Fig. 4b**). While EGFR-L858R-Cub-GAL4-NFkB displayed significantly higher Nub-Shc1-binding in serum-dependent and serum-independent conditions, the kinase-dead EGFR-D855A-Cub-GAL4-NFkB failed to bind Nub-Shc1, correlating with receptor phosphorylation patterns (**Fig. 4c**). Thus, MaMTH allows monitoring of PPIs that are dependent on the activity and phosphorylation state of a given receptor.

MaMTH can capture drug-inhibited interactions of oncogenic EGFR-variants

We further investigated EGFR-L858R and EGFR-exon 19 deletion (EGFR-ex19del), common oncogenic EGFR variants found in non-small cell lung cancer (NSCLC)[27, 28]. Lung cancer patients carrying these mutations are usually responsive to treatment with the tyrosine kinase inhibitor (TKI) erlotinib (Tarceva, OSI-774)[27]. We applied MaMTH to detect drug-inhibited PPIs through monitoring phosphorylation-dependent Shc1 recruitment to EGFR variants, in the presence and absence of erlotinib. MaMTH efficiently detected erlotinib-mediated inhibition of EGFR-L858R- and EGFR-ex19del-Cub-GAL4-NFkB and Nub-Shc1 interaction, while EGFR-Wt-Cub-GAL4-NFkB and Nub-Shc1 interaction was unaffected (**Supplementary Fig. 8a**). EGFR-ex19del-Cub-GAL4-NFkB showed decreased Nub-Shc1 binding at significantly lower erlotinib concentrations compared to EGFR-L858R-Cub-GAL4-NFkB (**Supplementary Fig. 8b**), consistent with the greater erlotinib sensitivity of EGFR-ex19del receptor reported previously[29]. NSCLC patients treated with erlotinib frequently develop a second EGFR-mutation (L858R/T790M), rendering the receptor unresponsive to erlotinib[28]. Strikingly, EGFR-L858R/T790M-Cub-GAL4-NFkB did not show decreased Nub-Shc1-binding upon erlotinib

treatment, behaving instead like EGFR-Wt-Cub-GAL4-NFkB, confirming its erlotinib-resistance (**Fig. 4d**). Mutant EGFR receptor baits were expressed at levels comparable to EGFR-Wt, displayed correct PM-localization plus/minus erlotinib (**Supplementary Fig. 8c-d** and **Fig. 4d**), and showed significantly higher basal Nub-Shc1-binding than EGFR-Wt-Cub-GAL4-NFkB (**Supplementary Fig. 8e**). Nub-Shc1 binding patterns of mutant receptor baits correlated with TF cleavage levels and EGFR-phosphorylation pattern (**Fig. 4d**). In order to rule out a nonspecific effect of erlotinib on Shc1 binding, we tested other phospho-dependent and -independent EGFR interactors plus/minus erlotinib and imatinib, a TKI that specifically targets Bcr-Abl[30], but not EGFR (**Supplementary Fig. 9**). Whereas all phospho-dependent interactor preys showed a bait binding pattern similar to that of Nub-Shc1 upon erlotinib treatment (**Supplementary Fig. 9a**), phospho-independent interactors bound all EGFR mutant baits independent of drug treatment (**Supplementary Fig. 9b)**. Imatinib did not affect any interaction (**Supplementary Fig. 9a-b**). Furthermore, we showed that erlotinib did not influence interactions of unrelated PPIs (**Supplementary Fig. 6b**). We next tested the binding of Nub-Grb2-R86M and Nub-Shc1-R175Q mutant preys, which cannot bind EGFR[31, 32] and, as expected, observed reduced interaction with EGFR (**Fig. 4e**). We then showed that EGFR-baits in our assay can be activated by EGF (**Supplementary Fig. 10**). EGFR-Wt-Cub-GAL4-NFkB showed increased Shc1 binding upon EGF treatment, whereas EGFR-L858R- and EGFR-ex19del-Cub-GAL4-NFkB baits were not responsive to EGF upon erlotinib-treatment. Note that basal reporter activation in starvation media is observed, since MaMTH is a reporter assay monitoring PPIs over time, via luciferase accumulation, rather than in real-time (**Supplementary Fig. 10**).

Identification of dynamic interaction partners of EGFR-Wt and EGFR-L858R

As lung cancer is the leading cause of cancer-related mortality worldwide[33], it is important to gain insight into PPIs of oncogenic receptors. We therefore upscaled MaMTH to characterize the differential interaction profiles of the oncogenic EGFR-L858R mutant versus EGFR-Wt.

We performed a targeted screen using 205 computationally predicted EGFR-interactors (**Supplementary Table 1**), of which 109 were previously identified EGFR-interactors (**Supplementary Table 2**). For detailed descriptions of EGFR-predictions, screening procedure and MaMTH interaction scores see Online Methods and **Supplementary Table 3**. Of 205 preys, 124 interacted with EGFR-Wt and/or EGFR-L858 (**Supplementary Table 4**). 67 of these bound more strongly to EGFR-L858R-Cub-GAL4-NFkB, 30 bound more strongly to EGFR-Wt-Cub-GAL4-NFkB and 27 showed comparable binding (**Supplementary Table 4**). The majority of preys binding more strongly to the mutant bait reflecting its increased phosphorylation-state and recruitment of phospho-dependent interactors. In summary, we detected 64.2% of known EGFR-interactors (70/109) and 54 previously uncharacterized EGFR-interactors (**Supplementary Table 4**). Among the 124 detected interactors, 13 are prognostic markers

for lung cancer (**Supplementary Table 4** and **Supplementary Fig. 11**), 9 of which showed a higher binding affinity to EGFR-L858R-Cub-GAL4-NFkBindicating that the mutant receptor binds more proteins involved in aberrant signaling. **Supplementary Fig. 12** shows a Venn diagram of proteins tested and detected or not detected by MaMTH. The majority of the 39 known interactors our screen did not detect were identified by co-immunoprecipitation-based studies, and thus might have been missed by our assay (**Supplementary Table 5**).

Validation of MaMTH interactors

As a secondary validation, a subset of PPIs from our dataset was tested using LUMIER[34, 35]. We selected 60 interactors based on whether (i) they showed significantly different binding in MaMTH to EGFR-Wt- and EGFR-L858R-Cub-GAL4-NFkB, (ii) are prognostic markers in lung cancer or (iii) have not previously been reported to interact with EGFR. Of 60 MaMTH interactors tested, 23 were LUMIER-positive (10/23 novel, 13/37 known). The binding patterns with EGFR-Wt and EGFR-L858R observed using LUMIER for 6 of these 23 positive interactors were similar to those displayed in MaMTH (**Fig. 5a** and **Supplementary Table 6**). As another validation, 17 of the 60 MaMTH interactors were tested by co-IPs and mass spectrometry (MS) (**Fig. 5a** and **Supplementary Figs. 13** and **14**). Of these, 13 were detected by co-IPs (**Supplementary Fig. 13**), and 9 by MS (**Supplementary Fig. 14**). Co-IPs confirmed 3/3 novel and 10/14 previously known EGFR interactors, while MS confirmed 2/3 novel and 7/14 previously known interactors. Overall, we showed that 11/23 (47.8%) of novel interactors and 34/60 (56.7%) of all tested interactors were confirmed by at least one orthogonal method.

Functional annotation of MaMTH hits: Novel roles of EGFR interactors in oncogenic signaling

We next examined the role on signaling pathways of interactors showing differential EGFR-binding. We compared the selected 60 MaMTH interactors with shRNA-knockdown data from erlotinib-sensitive HCC827 cells (NSCLC-cells harboring EGFR-ex19del). Briefly, HCC827 cells were infected with lentiviral shRNAs[36] and grown plus/minus erlotinib. shRNA abundance was compared and a relative drop-out rate calculated, indicating whether knockdown conferred a fitness disadvantage (depleted genes) or advantage (enriched genes) upon erlotinib treatment. Strikingly, knockdown of CRKII led to a drastic fitness defect in erlotinib-treated cells, reflected by the greatest negative drop-out rate among the 60 candidates (**Fig. 5a** and **Supplementary Table 7**). CRKII also interacted strongly with the oncogenic EGFR-L858R mutant in both MaMTH and LUMIER (**Fig. 5a**). These data suggested an active role of CRKII in cell survival or oncogenic signaling. CRKII and CRKL, belonging to the CRK family of adaptor proteins, are often found over-expressed in various cancers[37]. We tested the role of CRKII in oncogenic signaling, knocking it down and overexpressing it in HCC827

cells (**Fig. 5b-c**). Interestingly, whereas mock-infected HCC827 cells showed loss of phospho-ERK and phospho-AKT signaling upon erlotinib-treatment as expected (**Fig. 5b**), cells ovexpressing CRKII showed persistent phospho-ERK and phospho-AKT signaling in the presence of erlotinib, similar to the effect of overexpressed CRKL reported previously[38]. Moreover, increased EGFR levels were observed in HCC827 cells overexpressing CRKII, whereas the opposite effect was observed in EGFR-Wt-H226-cells (**Supplementary Fig. 15a-b**). This suggests that CRKII stabilizes or induces expression of the mutant receptor. CRKII-overexpression also improved viability of HCC827 cells in the presence of erlotinib, whereas CRKII knockdown led to increased erlotinib-sensitivity (**Fig. 5d**). We performed the same experiments with other interactors identified in the MaMTH screen, but no changes in phospho-ERK levels or cell viability were observed (**Supplementary Fig. 15c**). Taken together, we showed that CRKII overexpression induces oncogenic signaling and can partially bypass erlotinib-mediated sensitivity in HCC827 cells.

Discussion

Despite the variety of technologies available for use in identifying protein interactions, the study of physiological context-dependent membrane protein PPIs remains quite challenging. Although various PCAs[4, 10, 19] have been successfully applied to probe PPIs of ErbBs or GPCRs that change upon ligand/agonist-binding or phosphorylation, they have been limited to studies of a single protein or a limited protein subset[8-10].

Thus, the objective of developing MaMTH was to complement and improve upon existing techniques to allow for better identification of context-dependent interactions of full-length integral membrane proteins. Key MaMTH features include: **(i)** high transferability, allowing it to be carried out in virtually any cell line; **(ii)** compatibility with Gateway cloning technology; **(iii)** ability to detect subtle changes in interaction patterns in response to various stimuli; and **(iv)** amenability for high-throughput screening.

We showed that MaMTH can map phosphorylated residues on RTKs that mediate PPIs with adaptor proteins. Given that identification of phosphorylated docking sites of ErbB receptors has so far only been detectable by mass spectrometry-based methods[3], MaMTH offers a new cell-based platform to identify phospho-binding sites on integral membrane receptors. We also demonstrated how MaMTH allows monitoring of dynamic PPIs, specifically showing that MaMTH can identify the increased phosphorylation state of various oncogenic ErbB family members via measurement of adaptor protein recruitment. Plus, we could detect increased protein-recruitment to the erlotinib-resistant EGFR-L858R/T790M receptor[39], which could be used to identify novel pharmaceuticals directed towards acquired TKI-resistance[39].

In a first approach to upscale MaMTH for high-throughput applications, we performed a targeted screen to identify dynamic changes in PPIs of EGFR-wildtype and oncogenic EGFR-L858R mutant. We showed that MaMTH was able to robustly detect 64.2% of previously identified EGFR-interactors. Compared to a recent mass spectrometry-based study to generate a dynamic map of Wt and oncogenic EGFR variants[40], our approach is more likely to capture transient and weak interactions that vary slightly between wildtype and mutant. We identified 54 previously unknown EGFR-interactors, and validated 11/23 of these by two different orthogonal methods. We additionally characterized CRKII as a novel player in oncogenic EGFR signaling.

In summary, we present MaMTH as a novel technology to map dynamic interactions of human integral membrane proteins in modification-dependent contexts. As MaMTH operates in a multi-well format, it is easily adapted to large-scale formats and will soon be adapted to test small-molecule compounds that interfere with PPIs involved in cell signaling. We predict that MaMTH will help expand existing large-scale PPI analyses into multiple dimensions, probing interactome changes in response to drugs, hormones or different growth conditions. Ultimately, it should be a valuable tool in the identification of factors associated with aberrant signaling cascades, and aid greatly in the development of novel drug therapies to treat diseases associated with membrane protein dysfunction.

Acknowledgements

We would like to thank B. Andrews (Donnelly Centre, University of Toronto), C. Nislow (Department of Pharmaceutical Sciences, University of British Columbia), J. Moffat (Donnelly Centre, University of Toronto), M.-S. Tsao (Princess Margaret Cancer Centre, Toronto), B. Neel (Princess Margaret Cancer Centre, Toronto) for providing reagents and access to equipment; S. Angers, K. Blakely, J. Jin, S. Kittanakom, A. Arnoldo, M. Mendoza and Y. Fedyshyn for experimental assistance and advice; and U. Petrovic, M. Ali, M. Lam, Z. Yao, K. Sokolina for advice and/or critical review of the manuscript. This work was supported by grants from the Ontario Genomics Institute (303547), Canadian Institutes of Health Research (Catalyst-NHG99091, PPP-125785), Canadian Foundation for Innovation (IOF-LOF), Natural Sciences and Engineering Research Council of Canada (RGPIN 372393-12), Canadian Cystic Fibrosis Foundation (300348), Canadian Cancer Society (2010-700406), Novartis and University Health Network (GL2-01-018) to I. Stagljar. J. Petschnigg was a recipient of an FWF-Erwin Schrödinger postdoctoral fellowship.

Author contributions

I.S. conceived the project, provided guidance and assisted in manuscript preparation. J.P. coordinated, managed and was actively involved in all experiments, and wrote the bulk of the

manuscript. B.G. was actively involved in the design and performance of the functional and screening part of MaMTH. M.K., I.J. provided bioinformatics predictions and analysis of EGFR-interactors. M.T., I.K. and S.L. were responsible for LUMIER. Y.Z., T.P. generated co-IP and MS data. C.F.K. performed knockdown confirmations and provided technical help for all experiments. A.S., J.R.S., M.-S.T., J.M. generated and analysed shRNA knockdown data. J.S. was actively involved in manuscript preparation and provided project guidance. M.M.U., and A.N. were involved in data analysis, bait/prey generation and fluorescence microscopy. All authors discussed the results and commented on the manuscript.

Competing Financial Interests Statement

The authors declare competing financial interests. A provisional patent application was filed by the University of Toronto on July 2nd 2013 to the U.S. Patent and Trademark Office, Application # 61/833,304. The intellectual property has been assigned to the University of Toronto and its commercialization is being managed by the Innovations and Partnership Office.

References

1. Stevens, T.J. & Arkin, I.T. Do more complex organisms have a greater proportion of membrane proteins in their genomes? *Proteins* **39**, 417-420 (2000).
2. Jones, R.B., Gordus, A., Krall, J.A. & MacBeath, G. A quantitative protein interaction network for the ErbB receptors using protein microarrays. *Nature* **439**, 168-174 (2006).
3. Schulze, W.X., Deng, L. & Mann, M. Phosphotyrosine interactome of the ErbB-receptor kinase family. *Mol Syst Biol* **1**, 2005.0008 (2005).
4. Lievens, S., Lemmens, I. & Tavernier, J. Mammalian two-hybrids come of age. *Trends Biochem Sci* **34**, 579-588 (2009).
5. Michnick, S.W., Ear, P.H., Manderson, E.N., Remy, I. & Stefan, E. Universal strategies in research and drug discovery based on protein-fragment complementation assays. *Nat Rev Drug Discov* **6**, 569-582 (2007).
6. Rojo-Niersbach, E., Morley, D., Heck, S. & Lehming, N. A new method for the selection of protein interactions in mammalian cells. *Biochem J* **348 Pt 3**, 585-590 (2000).
7. Kerppola, T.K. Visualization of molecular interactions by fluorescence complementation. *Nat Rev Mol Cell Biol* **7**, 449-456 (2006).
8. Stefan, E. et al. Quantification of dynamic protein complexes using Renilla luciferase fragment complementation applied to protein kinase A activities in vivo. *Proc Natl Acad Sci U S A* **104**, 16916-16921 (2007).
9. Wehrman, T.S. et al. A system for quantifying dynamic protein interactions defines a role for Herceptin in modulating ErbB2 interactions. *Proc Natl Acad Sci U S A* **103**, 19063-19068 (2006).
10. Wehr, M.C. et al. Monitoring regulated protein-protein interactions using split TEV. *Nat Methods* **3**, 985-993 (2006).
11. Ciruela, F. Fluorescence-based methods in the study of protein-protein interactions in living cells. *Curr Opin Biotechnol* **19**, 338-343 (2008).
12. Johnsson, N. & Varshavsky, A. Split ubiquitin as a sensor of protein interactions in vivo. *Proc Natl Acad Sci U S A* **91**, 10340-10344 (1994).
13. Stagljar, I., Korostensky, C., Johnsson, N. & te Heesen, S. A genetic system based on split-ubiquitin for the analysis of interactions between membrane proteins in vivo. *Proc Natl Acad Sci U S A* **95**, 5187-5192 (1998).
14. Paumi, C.M. et al. Mapping protein-protein interactions for the yeast ABC transporter Ycf1p by integrated split-ubiquitin membrane yeast two-hybrid analysis. *Mol Cell* **26**, 15-25 (2007).
15. Snider, J. et al. Mapping the functional yeast ABC transporter interactome. *Nat Chem Biol* **9**, 565-572 (2013).
16. Emami, K.H. & Carey, M. A synergistic increase in potency of a multimerized VP16 transcriptional activation domain. *Embo J* **11**, 5005-5012 (1992).
17. Sadowski, I., Ma, J., Triezenberg, S. & Ptashne, M. GAL4-VP16 is an unusually potent transcriptional activator. *Nature* **335**, 563-564 (1988).
18. Schmitz, M.L. & Baeuerle, P.A. The p65 subunit is responsible for the strong transcription activating potential of NF-kappa B. *Embo J* **10**, 3805-3817 (1991).
19. Remy, I. & Michnick, S.W. Application of protein-fragment complementation assays in cell biology. *Biotechniques* **42**, 137, 139, 141 passim (2007).
20. Johnsson, N. & Varshavsky, A. Ubiquitin-assisted dissection of protein transport across membranes. *Embo J* **13**, 2686-2698 (1994).
21. Rhee, Y., Gurel, F., Gafni, Y., Dingwall, C. & Citovsky, V. A genetic system for detection of protein nuclear import and export. *Nat Biotechnol* **18**, 433-437 (2000).
22. Deribe, Y.L. et al. Regulation of epidermal growth factor receptor trafficking by lysine deacetylase HDAC6. *Sci Signal* **2**, ra84 (2009).
23. Moore, C.A., Milano, S.K. & Benovic, J.L. Regulation of receptor trafficking by GRKs and arrestins. *Annu Rev Physiol* **69**, 451-482 (2007).

24. DeWire, S.M., Ahn, S., Lefkowitz, R.J. & Shenoy, S.K. Beta-arrestins and cell signaling. *Annu Rev Physiol* **69**, 483-510 (2007).
25. Yarden, Y. & Sliwkowski, M.X. Untangling the ErbB signalling network. *Nat Rev Mol Cell Biol* **2**, 127-137 (2001).
26. Prickett, T.D. et al. Analysis of the tyrosine kinome in melanoma reveals recurrent mutations in ERBB4. *Nat Genet* **41**, 1127-1132 (2009).
27. da Cunha Santos, G., Shepherd, F.A. & Tsao, M.S. EGFR mutations and lung cancer. *Annu Rev Pathol* **6**, 49-69 (2011).
28. Pines, G., Kostler, W.J. & Yarden, Y. Oncogenic mutant forms of EGFR: lessons in signal transduction and targets for cancer therapy. *FEBS Lett* **584**, 2699-2706 (2010).
29. Carey, K.D. et al. Kinetic analysis of epidermal growth factor receptor somatic mutant proteins shows increased sensitivity to the epidermal growth factor receptor tyrosine kinase inhibitor, erlotinib. *Cancer Res* **66**, 8163-8171 (2006).
30. Shortt, J. & Johnstone, R.W. Oncogenes in cell survival and cell death. *Cold Spring Harb Perspect Biol* **4** (12) (2012).
31. Ahn, R. et al. The ShcA PTB domain functions as a biological sensor of phosphotyrosine signaling during breast cancer progression. *Cancer Res* **73**, 4521-4532 (2013).
32. Bisson, N. et al. Selected reaction monitoring mass spectrometry reveals the dynamics of signaling through the GRB2 adaptor. *Nat Biotechnol* **29**, 653-658 (2011).
33. Jemal, A. et al. Cancer statistics, 2009. *CA Cancer J Clin* **59**, 225-249 (2009).
34. Barrios-Rodiles, M. et al. High-throughput mapping of a dynamic signaling network in mammalian cells. *Science* **307**, 1621-1625 (2005).
35. Taipale, M. et al. Quantitative analysis of HSP90-client interactions reveals principles of substrate recognition. *Cell* **150**, 987-1001 (2012).
36. Blakely, K., Ketela, T. & Moffat, J. Pooled lentiviral shRNA screening for functional genomics in mammalian cells. *Methods Mol Biol* **781**, 161-182 (2011).
37. Sriram, G. & Birge, R.B. Emerging roles for crk in human cancer. *Genes Cancer* **1**, 1132-1139 (2010).
38. Cheung, H.W. et al. Amplification of CRKL induces transformation and epidermal growth factor receptor inhibitor resistance in human non-small cell lung cancers. *Cancer Discov* **1**, 608-625 (2011).
39. Kosaka, T., Yamaki, E., Mogi, A. & Kuwano, H. Mechanisms of resistance to EGFR TKIs and development of a new generation of drugs in non-small-cell lung cancer. *J Biomed Biotechnol* **2011**, 165214 (2011).
40. Li, J. et al. Perturbation of the mutated EGFR interactome identifies vulnerabilities and resistance mechanisms. *Mol Syst Biol* **9**, 705 (2013).

Figure legends

Figure 1. Set-up and validation of the Mammalian-Membrane-Two-Hybrid (MaMTH) system.

a) MaMTH detects transcriptional activation of luciferase or GFP reporter genes located downstream of 5xGAL4UAS- or 8xlexAops-DNA-binding sites. The integral membrane protein-Cub-TF bait and Nub-prey (either membrane or cytosolic protein) are co-transfected (or infected) into HEK293T cells stably expressing the reporter genes. Upon bait and prey interaction, ubiquitin reconstitution occurs, leading to the proteolytic cleavage by deubiquitinating enzymes (DUBs), and the subsequent release of the transcription factor (TF). The TF enters the nucleus resulting in reporter gene activation.

b) Known interactions between ErbB4-Cub-GAL4-NFkB/ErbB4-Cub-mLexA-VP16 and Nub-Grb2 or Nub-Shc1 could be reconstituted in stable 5xGAL4UAS-luciferase and 8xlexA-ops-luciferase HEK293T reporter cells and showed luciferase activity above the negative prey control (Nub-Fabp5). Reporter gene activation was followed by Western Blot using VP16 antibody or V5 antibody. Prey expression was assessed using Flag-antibody. Error bars indicate standard deviation (*n = 3*). Statistical significance is shown by asterisks *** $p < 0.001$, ** $p < 0.01$.

c) Stable bait/luciferase-5xGAL4UAS-luciferase reporter HEK293T cell lines were infected with positive and negative control preys and 4 days after infection, cells were lysed and subjected to luciferase assays. Known interactions with Nub-Grb2, -Shc1 and -Hsp90 were successfully reconstituted. Additionally, both ErbB4- and EGFR-baits interacted with Nub-GAPDH and Nub-Cfl1. Error bars indicate standard deviation (*n = 3*). Statistical significance is shown by asterisks *** $p < 0.001$, ** $p < 0.01$.

Figure 2. Using MaMTH to monitor agonist-dependent interactions of β2-AR and β-arrestin.

a) β2-AR-Cub-mLexA-VP16-bait and Nub-β-arrestin-prey were co-transfected into stable 8xlexAops-luciferase reporter cells, treated with or without agonist for 4-12 h and luciferase assays were performed. An increase in luciferase expression after 4-8 h agonist addition indicated elevated levels of activated receptor bait and increased β-arrestin recruitment. Relative luciferase activity is based on fold-change increase above the control (bait only). Error bars indicate standard deviation (*n = 3*). Statistical significance is denoted by asterisks *** $p < 0.001$, ** $p < 0.01$.

b) β2-AR-Cub-GFP-mLexA-VP16 baits were transfected into reporter cells and fluorescence microscopy was performed using a plasma membrane (PM) stain (Deep Red, CellMask). Scale bar = 10μM.

c) β2-AR-Wt- and mutant-Cub-mLexA-VP16 baits lacking GRK6-, GRK2 or GRK2 and GRK6-phosphorylation sites were co-transfected with Nub- β-arrestin prey into stable 8xlexAops-luciferase HEK293T reporter cells, treated with agonist for 8 h and luciferase assays were performed. β2-AR-

bait lacking GRK2 and GRK6 phospho-sites showed no agonist-induced increase in β-arrestin binding, comparable to untreated condition. Fold-change increase above bait control is shown. A fraction of the lysates was subjected to Western Blot analysis. Error bars indicate standard deviation (*n = 3*). Statistical significance is denoted by asterisks *** $p < 0.001$, ** $p < 0.01$.

d) β2-AR-Wt- and β2-AR-GRK6/GRK2-Cub-mLexA-VP16-baits and Nub- β-arrestin or Nub- β-arrestin -R169E mutant prey were co-transfected into HEK293T stable 8xlexAops-luciferase reporter cells, treated with agonist and luciferase assays were performed. Relative luciferase activity is based on fold-change increase above the bait control. A fraction of the lysates was subjected to Western Blot analysis. Error bars indicate standard deviation (*n = 3*). Statistical significance is denoted by asterisks ** $p < 0.01$.

Figure 3. MaMTH allows sensitive detection of PPIs involving Y-X-N Grb2 binding sites in ErbB family members.

a) Stable 5xGAL4UAS-luciferase reporter cells were co-transfected with EGFR-Wt- or phospho-site mutant-Cub-GAL4-NFkB baits (Y1092A or Y1092A/Y1138A) and Nub-Grb2, Nub-CRKII or Nub-GAPDH. Luciferase activity was measured 24h following transfection and is shown as fold-change difference compared to EGFR-Wt-Cub-GAL4-NFkB. A fraction of lysates was subjected to Western blot analysis using anti-V5 (bait expression and cleaved off TF), anti-flag (prey expression) and anti-tubulin antibodies. Error bars indicate standard deviation (*n = 3*). Statistical significance is denoted by asterisks ** $p < 0.01$, * $p < 0.05$.

b) Ligand-dependent interaction of ErbB2-Cub-GAL4-NFkB ErbB3-Cub-GAL4-NFkB with Nub-Grb2 (left panel) and Nub-Shc1 (right panel). Following overnight starvation, cells transiently expressing ErbB3- or ErbB2--Cub-GAL4-NFkB baits (Wt or mutated in specific Y-residues) were treated with 10ng/ml Neuregulin for 4 h, followed by luciferase activity measurement. A fraction of the lysates was subjected to Western blot analysis using anti-V5 (bait expression and cleaved off TF), anti-flag (prey expression) and anti-tubulin antibodies. Error bars indicate standard deviation (*n = 3*). Statistical significance is denoted by asterisks *** $p < 0.001$, * $p < 0.05$.

Figure 4. Monitoring phosphorylation-dependent interactions of oncogenic ErbB family members.

a) Stable 5xGAL4UAS-luciferase cells were co-transfected with indicated ErbB4-baits and Nub-Shc1, grown -/+ serum followed by luciferase measurement. Oncogenic baits showed increased Nub-Shc1 binding compared to Wt. Relative luciferase activity shows fold-change difference compared to ErbB4-Wt. A fraction of the starvation lysates was subjected to Western blot analysis. Error bars indicate standard deviation (*n = 3*). Statistical significance is denoted by asterisks ** $p < 0.01$, * $p < 0.05$.

b) Experiment was performed as in **a)**

c) Stable 5xGAL4UAS-luciferase cells were co-transfected with EGFR-baits and Nub-Shc1, grown -/+ serum followed by luciferase measurement. Receptor expression and phosphorylation patterns were assessed by Western Blot using anti-V5 (FBS-treated cell lysates) and phospho-tyrosine(pTyr)-specific antibodies (Flag-tagged-immunoprecipitated EGFR-samples). Error bars indicate standard deviation (*n = 3*). Statistical significance is denoted by asterisks *** $p < 0.001$, ** $p < 0.01$, * $p < 0.05$.

d) Stable 5xGAL4UAS-luciferase cells were co-transfected with indicated baits and Nub-Shc1, treated with erlotinib followed by luciferase measurement. Untreated controls were set to 1 and fold-changes in luciferase activity are shown. A fraction of the lysates was subjected to Western blot analysis. Error bars indicate standard deviation (*n = 3*). Statistical significance is denoted by asterisks *** $p < 0.001$.

e) EGFR baits were co-transfected with Nub-Shc1 and Nub-Grb2 or Nub-Shc1-R175Q and Nub-Grb2-R86M, treated with erlotinib followed by luciferase measurement. Luciferase activity shows fold-change difference compared to untreated control. A fraction of the lysates was subjected to Western blot analysis. Error bars indicate standard deviation (*n = 3*). Statistical significance is denoted by asterisks ** $p < 0.01$.

Figure 5. Confirmation of MaMTH interactors and involvement of CRKII in cancer signaling

a) Confirmation of 60 MaMTH-interactors (23 novel and 37 known) by LUMIER, co-IP and MS. X- and Y-axes show MaMTH interaction-scores**.** The dotted line separates interactors binding stronger to EGFR-Wt (x-axis) or EGFR-L858R (y-axis). 10/23 novel interactors were confirmed by LUMIER, 6/23 showed similar EGFR-binding pattern as MaMTH (green triangle). Out of 17 tested MaMTH-interactors, co-IPs detected 3/3 novel and 10/14 known interactors (pink triangle). MS detected 2/3 novel interactors and 7/14 known interactors (orange triangle). 11/23 novel and 34/60 previously known and novel interactors were confirmed by orthogonal assays.

Downward triangles indicate that knockdown of the gene led to less survival of HCC827-cells (negative drop-out rate), upward triangles indicate that knockdown of that gene increased fitness of erlotinib-treated HCC827-cells (positive drop-out rate). Triangle size shows FDR (false-discovery rate) values.

b) HCC827-cells infected with indicated lentiviruses were treated with EGF or treated with erlotinib and EGF-stimulated. Cells were lysed and immunoblotting performed with indicated antibodies.

c) Confirmation of CRKII, PDGFRA and MUC1 expression. Knockdowns of genes were confirmed by qPCR compared to GFP-control cells. Data are presented as means ± standard deviation (*n = 3*), Statistical significance is denoted by asterisks *** $p < 0.001$, ** $p < 0.01$.

d) Cell viability assays were performed in erlotinib-treated HCC827-cells with overexpressed or knocked-down CRKII or PDGFRA. Values are relative to the control-shGFP. Data are presented as means ± standard deviation (*n = 3*), Statistical significance is denoted by asterisks *** $p < 0.001$, ** $p < 0.01$.

Online Methods

Bait, prey and reporter plasmid construction

Supplementary Table 8 shows a complete list of plasmid backbones used in this study. **Supplementary Table 9** shows primers used to generate reporters, baits and preys.

Gateway-compatible entry clones: Entry clones were obtained by the human ORFeome library v8.1[41] or PCR-amplified from Mammalian Gene Collection clones to create entry clones in pDONR223 using Gateway BP cloning technology (Invitrogen) according to the manufacturer's protocol. Entry clones were sequence-verified.

MaMTH reporter vectors: Lentiviral reporter constructs were constructed using pLD-Gateway-Puro-NVF (kind gift of Dr. Kim Blakely and Dr. Jason Moffat) as a backbone, which was cut with BstBI and KpnI to remove the Puromycin marker. The cPPT-hPGK-Hygro-resistance marker cassette (amplified from pLD-hygro-EcMV, kind gift of Kim Blakely and Jason Moffat) was PCR-amplified with flanking BstBI/KpnI sites and ligated into the cut vector. The resulting vector was cut with SanDI and SalI and the insert 5xGAL4UAS (upstream-activating sequence)-TATA-box-luciferase (PCR-amplified from template pFR-Luc, Stratagene) was ligated into the vector. The resulting 5xGAL4UAS-TATA-box-luciferase-hygromycin-plasmid was cut with SanDI and BamHI to replace the 5xGAL4UAS-sites with 8xlexAops-sites (PCR-amplified from plasmid L8-Luc[42]). 5xGAL4UAS-TATA-box-luciferase-hygromycinR and 8xlexAops-TATA-box-luciferase-hygromycinR -plasmids were then used to excise luciferase and clone eGFP into BamHI/SalI sites (eGFP was amplified from template pLJM1). Final constructs were sequence-verified.

MaMTH-bait and prey destination vectors: Bait and prey destination vectors were generated using standard restriction digest and T4 ligation protocols. Combinations of Cub-transcription factor inserts were generated by homologous recombination in yeast: briefly, regions of Cub, DNA-binding domain and transcriptional activation domain were PCR-amplified (for templates see below) with overhangs complementary to the yeast vector backbone pCCW-Ste or the adjacent inserts. pCCW-Ste was cut with NotI/FspI and up to 3 inserts (Cub, DBD, AD) were co-transformed into yeast BY4742 using standard Lithium acetate transformation. Recombined constructs were then sequenced and the inserts "Cub-TF" were PCR-amplified containing 1) linker regions and 2) restriction sites suitable for cloning the tags into mammalian vector backbones to generate final destination vectors. Final bait destination vectors are based on pGateway-CMV5'-tripleFLAG or pGateway-CMV3'-tripleFLAG (kind gifts of Jason Moffat's lab), and the tags "linker-Cub-mLexA-VP16" or "linker-Cub-GAL4-mNFkB" were cloned into XbaI sites of pGateway-CMV5'-tripleFLAG to obtain MaMTH bait destination vectors for C-terminal tagging. Final prey destination vectors are also based on pGateway-CMV5'-tripleFLAG or pGateway-CMV3'-tripleFLAG, and linker-tripleFLAG-Nub were cloned into XbaI site of pGateway-CMV5'-tripleFLAG to obtain MaMTH prey vectors for C-terminal tagging or Kozak-Nub-tripleFLAG-

linker was cloned into KpnI/HindIII sites of pGateway-CMV3'-tripleFLAG to obtain MaMTH prey vectors for N-terminal tagging. Lentiviral prey backbones were based on pLD-Gateway-Puro-CVF and pLD-Gateway-Puro-NVF (kind gifts of Kim Blakely and Jason Moffat), and linker-tripleFLAG-Nub was cloned into EcoRV/BstBI sites of pLD-Gateway-Puro-CVF to obtain MaMTH lentiviral prey destination vectors for C-terminal tagging or Kozak-Nub-tripleFLAG-linker was cloned into EcoRV/NheI sites of pLD-Gateway-Puro-NVF to obtain MaMTH lentiviral prey destination vectors for N-terminal tagging.
Prey linker regions were introduced by incorporating linkers into primers. C-terminal ubiquitin (aa 35-76) and N-terminal ubiquitin (aa 1-37) was PCR-amplified from yeast genomic DNA (for yCub and yNubi) or from human ubiquitin-cDNA (for hCub and hNubi). Regions after yCub or hCub was amplified from MYTH-TMBValpha and contains a 5'-ATG (ATGcacagatcagcttgcggccgc) to ensure that the cleaved off transcription factor is not degraded according to the N-end rule. Variants of yNub or hNub were generated using site-directed mutagenesis protocols (Stratagene). All MaMTH bait and prey destination vectors were fully sequenced, and expression clones (after LR reaction of entry clones with the respective destination vectors) were sequenced at the junctions between bait- or prey-tags and cDNAs. Bait and prey expression vectors were created using Invitrogen LR cloning technology with entry clones mentioned above and self-designed destination vectors.
MaMTH-vectors for testing performance: Chimeric transcription factors used in **Supplementary Fig. 1a** were PCR-amplified from mouse-RELA-cDNA (mNFkB), human RELA-cDNA (hNFkB), GAL4-DBD (pDEST32 Invitrogen), MYTH-vectors pTMBValpha (LexA and VP16) and pNIA E432 #40 (mLexA[21]) and standard restriction digests and T4-ligation were performed. Chimeric transcription factors were ligated into pGateway-CMV3'-tripleFLAG cut with KpnI and XbaI, where the Gateway cassette was taken out. Mutants of ErbB family members and ß2-AR were generated by site-directed mutagenesis and sequence-verified in full. GFP-constructs for bait localization were constructed by homologous recombination in yeast (final inserts Cub-GFP-mLexAVP16 or Cub-GFP-GAL4-NFkB) and then PCR-amplified with XbaI-restriction sites and ligated into pGateway-CMV5'-tripleFLAG cut with XbaI to generate C-terminally tagged bait-GFP destination vectors.

Lentivirus generation

Lentiviral reporter or prey plasmids were co-transfected with psPAX2 and pMD2 into HEK293T cells using X-tremeGene9 transfection reagent (Roche) and Optimem-serum-reduced media (Gibco). 18h after transfection, media was removed and replaced by viral harvesting media (DMEM+1.1g/100mL BSA). 24 h later, the first viral harvest was performed and high-BSA harvesting media added to the cells. Again after 24 h, the second harvest was done and combined with the first harvest and virus was stored at -80°C. Lentiviral work was carried out in accordance with all Biosafety requirements.

Stable cell line generation

Lentiviral titers were assayed and target cells were infected at a multiplicity of infection between 0.3-0.5. 24 h after infection, cells were selected with puromycin (2 µg/ml for HEK293T, 1.5 µg/ml for HCC827, H226) in case of infection with preys, overexpression constructs or shRNAs for at least 48h and expanded or frozen down for further assays. In case of infection with reporter constructs, cells were selected with hygromycin (100 µg/ml for HEK293T) for at least 7-10 days, and single cells were isolated by limited dilution. Briefly, stable reporter cells were seeded into 96-well plates that on average each well contained one cell. About 7 days later, colonies were expanded and assayed for reporter gene activation. Clones that gave high luciferase signal upon transfection with full-length transcription factors compared to negative controls were expanded and used for further experiments. Double bait/reporter double stable cell lines were generated through transfection, as bait-lentiviral constructs exceeded the lentiviral packaging limit and gave low virus titer. To this end, MaMTH-baits were co-transfected with a linear puromarker (Clontech) at a ratio 20:1 and selected in puromycin (2 µg/ml) 48 h after transfection for about 7 days. Single colonies were isolated using sterile cylinders and tested for bait expression by Western blot.

Cell culture

HEK293T cells were cultured in Dulbecco's modified Eagle's medium (DMEM) with 10 % fetal bovine serum and 1% antibiotics (penicillin/streptomycin). Lung cancer cell lines HCC827 and H226 were maintained in RPMI-1640 supplemented with 10 % fetal bovine serum and antibiotics. Starvation conditions were performed in DMEM or RPMI without FBS or with 0.1 % FBS. Erlotinib (kind gift of Dr. Ming-Sound Tsao) and imatinib (kind gift of Dr. Benjamin Neel's lab) were added at indicated concentrations, agonist isoproterenol (Sigma-Aldrich) was added at a concentration of 10 µM, TKI-PD158780 (Sigma-Aldrich) was added at 2 µM, Neuregulin (Cell Signaling Technology) was added at 5-10 nM.

Cell viability assay

HCC827 cells were seeded into white 96-well plates at 6000 cells/well. 24 h later, media was replaced with indicated concentrations of erlotinib, and 48 h afterwards, alamar blue (Invitrogen) was added to the media (10µl/well). After 3-4 h, absorbance was measured at 570nm and 600nm and cell viability calculated relative to untreated control wells.

Transfection experiments

Transfection experiments were performed using a modified calcium phosphate method. Briefly, for a 12-well plate, 65 µl ddH_2O and 75 µl 2xBES (N,N-bis(2-hydroxyethyl)-2-aminoethanesulfonic acid) were added to the DNA and 7,5 µl 2.5M $CaCl_2$ was then added and the tubes vortexed and incubated at room temperature for 15 minutes and added dropwise to the cells. 8-16 h later, the transfection mix was removed and replaced with indicated media.

MaMTH luciferase interaction assays

Firefly luciferase activity was measured as follows: infected or transfected reporter cells were lysed between 20 h (for drug treatments) or 48 h after transfection (expression analysis) or 4 days after infection. Wells were washed with PBS and Promega reporter lysis buffer (1x) plus protease inhibitor (Complete-EDTA-Roche) was added. Plates were frozen at -80°C to ensure complete lysis. Luciferase activity was measured from at least three independent experiments. Cell lysates were then measured on an injectable Berthold luminometer suitable for 96-wells plates. Luciferase experiments were performed at least in triplicates, and significance was based on *p*-values after two-tailed unpaired t-test calculations compared to corresponding controls.

For the EGFR-interaction screen, 205 top-predicted EGFR-interactors were cloned into lentiviral prey backbones. After lentivirus generation, target cells (stable 5xGAL4UAS-luciferase reporter-HEK293T cells) were infected with prey viruses in triplicates (C- or N-terminally tagged, depending on their cellular localization) at a multiplicity of infection (MOI) of around 0.3-0.4 to ensure single copy integration per cell. Cells were selected in puromycin for at least 48h, cell counts were performed and equal amounts of cells were transfected with EGFR-Wt or EGFR-L858R baits in triplicates. 24h after transfection, cells were lysed, cell counts and luciferase assays performed. Note that baits had to be transfected due to increased cell death upon stable integration of EGFR-L858R-Cub-GAL4-NFkB into reporter cells. Background luminescence was defined by a set negative control preys for each round of experiments. Negative controls were chosen from literature such that the proteins have previously not been reported to interact with the baits (Nub-Fabp5, Nub-Pex7, ABCD2-Nub, Nub-Pex19, GABBR2-Nub, Nub-KCTD6, Nub-FKBP12, Clcn5-Nub). Mann-Whitney U tests were used to assess whether luciferase activity from bait-prey interactions was significantly higher than from the same baits paired with negative control preys. Each test compared 3 luciferase activity measurements from a bait-prey pair (3 replicate experiments) against 24 measurements from the same bait and 8 negative controls (3 replicate experiments for each control). Positive MaMTH interactors were then re-tested with GABBR1 as an unrelated bait protein to exclude spurious preys. The MaMTH interaction ratios depict the ratios of interactor versus averaged negative controls. The ratio between EGFR-Wt and EGFR-L858R was then calculated for each bait-prey pair to depict

changes in interaction patterns between EGFR-Wt and EGFR-L858R. **Supplementary Table 3** provides luciferase data for the EGFR-screen and the unrelated bait interaction data.

Antibodies and Western blot analysis

Western blot analysis was performed using standard protocols. Briefly, cells were directly harvested in 2xsample buffer +ß-mercaptoethanol (2xSB) or harvested in 1xreporter lysis buffer (Promega) containing protease inhibitors (Complete-EDTA, Roche) and 2xSB was added after freezing the cells at -80°C. For phospho-specific antibodies, cells were lysed in Ripa buffer containing Na-orthovanadate, PMSF and protease inhibitor and 2xSB was added and samples were immediately boiled at 95°C for 5 min and proceeded for Western Blot analysis. 5-10 % of the lysates were separated by 10% SDS-PGE gels and transferred to nitrocellulose membranes. Transferred samples were immunoblotted with primary antibodies, followed by incubation with HRP-coupled secondary antibodies, and detection was performed using GE-Healthcare enhanced luminescence. A list of antibodies and dilutions used can be found in **Supplementary Table 10**.

Fluorescence microscopy

Bait constructs (harboring Cub-GFP-mLexA-VP16) were transfected into stable 8xlexAops-luciferase cells seeded on poly-L-lysine-coated glass slips. 48 h after transfection, fluorescence microscopy was performed. Cells were washed with warm PBS and covered in 5 µg/ml Invitrogen CellMask Deep Red dye for 5 minutes at 37°C. Cells were washed 3 times with warm PBS and immediately used for microscopy. Cells were examined using a Leica DMI 6000 B microscope with GFP and Texas Red. Images were analyzed using the Volocity software.

RNA extraction and qPCR for knockdown confirmation

RNA was prepared using the RNeasy minikit (Qiagen). QuantiTect Reverse Transcription kit (Qiagen) was used to eliminate genomic DNA and synthesize cDNA from up to 1 mg of RNA. qPCR reactions were performed on a Roche LightCycler 400 using a DyNAmo Flash SYBR Green qPCR kit (Thermo Scientific). Primer annealing was 35 seconds at 50°C and extension was 35 seconds at 72°C[43].

LUMIER assay

HEK293T cells were transfected in 96-well plates with EGFR-Renilla or EGFR-L858R-Renilla fusion constructs together with 60 selected 3xFlag-tagged bait plasmids. One day after transfection, normal growth medium (DMEM+10 %FBS) was replaced by low serum medium (DMEM+0.1 %FBS) for 16 h.

Cells were treated with 100ng/ml EGF or left untreated for 15 minutes before cell lysis. LUMIER assay was performed as described previously[35], except that interactions were not normalized to the bait protein abundance. LUMIER was performed in duplicates in three independent rounds. Significant interactors were based on *p*-values after t-test calculations compared to corresponding backgrounds.

EGFR predictions

EGFR interactors were computationally predicted using a data-mining based method, FpClass, which integrates diverse PPI evidence, including features that comprehensively characterize individual proteins and protein pairs. Features of individual proteins comprise domains, post-translational modifications, physico-chemical properties, localization, function and process. The probability of interaction depends on pairs of these features possessed by candidate interacting proteins; for example, interaction probability increases if proteins possess complementary domains that can facilitate binding. A pair of features increases (decreases) the probability of interaction if it is significantly enriched (deficient) among experimentally validated physical PPIs from the Interologous Interaction Database ver. 2.0 (I2D; http://ophid.utoronto.ca/i2d)[44]. The following features of protein pairs are also used as evidence for interaction: high co-expression of the genes encoding the protein pair, known interactions of orthologous or paralogous protein pairs, and shared interaction partners in a network of experimentally validated PPIs from I2D. Evidence from all features is integrated into a single probability of interaction. The method and its application to predicting human interactome orphans is described (Kotlyar M., Pastrello C., Lo Sardo A., Niu Y., Ding Z., Vafaee F., Broackes-Carter F., Mills G.B., Maestro R., & Jurisica I. Systematically characterizing human proteins without reported interactions, under review, 2013). Source for prognostic signatures: Lung prognostic signatures were downloaded from the LCDIP database (data not shown), which includes signatures from[45] and other sources.

Validation of novel EGFR interactions by co-immunoprecipitation and immunoblotting

HEK293T cells were seeded at 5 x 10^5 cells/well in a 6-well dish in DMEM + 10 % FBS. The following day, cells were co-transfected with FLAG-tagged candidate EGFR interactors and GFP-tagged EGFR. 24-hour post-transfection, cells were stimulated with EGF (100 ng/ml) for 5min, washed twice with ice-cold PBS, and lysed in 500 µl NP40 lysis buffer (50 mM HEPES-NaOH (pH 8), 150 mM NaCl, 1 mM EGTA, 0.5% NP40, 100 mM NaF, 2.5 mM $MgCl_2$, 10 mM $Na_4P_2O_7$, 1 mM dithiothreitol (DTT), 10% glycerol) supplemented with protease and phosphatase inhibitors (50 mM β-glycerolphosphate, 10 µg/ml aprotinin, 10 µg/ml leupeptin, 1 mM Na_3VO_4, 100nM calyculin A, 1 mM PMSF). The total cell lysates were centrifuged at 20,800 x g for 30 minutes to pellet the nuclei and insoluble material. Nuclear-free lysates were pre-cleared by one-hour incubation with protein A sepharose and

normalized for total protein concentration using the Bio-Rad protein assay. FLAG-tagged candidate proteins were immunoprecipitated by incubating lysates with 5 µl (bed volume) anti-FLAG M2 antibody-conjugated agarose for 4 hours at 4^{o}C. The beads were washed 4 times with lysis buffer. Co-immunoprecipitating proteins were resolved on 10% SDS-PAGE. Levels of GFP-EGFR were detected by immunoblotting using anti-GFP antibodies.

Validation of novel EGFR interactions by co-immunoprecipitation and mass spectrometry

5 x 106 HEK293T cells were co-transfected in a 10 cm tissue culture dish with FLAG-tagged candidate EGFR interactors and GFP-tagged EGFR for 24 hours. GFP-tagged EGFR was affinity purified using GFP Trap coupled to agarose (ChromoTek). The beads were washed 4 times with lysis buffer and twice with 50 mM ABC before resuspending in 20 µl ABC (50 mM). Tryptic digestion was performed by directly adding trypsin (enzyme: substrate~1:50) to the beads and incubating at 37°C overnight. The digestion was stopped by adding 3 % formic acid to the reaction and the supernatant was transferred into a clean tube and dried.

Dried tryptic samples were reconstituted with 3% formic acid in HPLC grade water. Samples were loaded on to a 75 µm ID/360 µm OD pulled tip packed with 3 µm ReproSil C18 and analyzed on an TripleTOF 5600 mass spectrometer (AB SCIEX) coupled to an Eksigent nanoLC Ultra 1D plus pump with a flow rate of 200 nl/min and a gradient of 2% to 35% acetonitrile over 90 min. The mass spectrometers were operated in information-dependent acquisition mode. A cycle time of 1.3 seconds was employed using a survey TOF scan of 250 millisecond (msec) at ~30,000 resolution followed by selection of the top 20 most intense peptides for MS/MS for 50 msec each with high sensitivity (at ~ 18,000 resolution). Only peptides with a charge state above +1 were selected for MS/MS and dynamic exclusion was set to 15 seconds for all ions within 20 ppm.

shRNA-knockdown screens and data analysis

Following the protocol detailed by Marcotte et al.[46], pooled shRNA screen measurements were performed at three time-points (t0, t1, t2), each in triplicate, for HCC827 cell with or without Erlotinib. T0 measurements were common to both conditions. A linear mixed model regression was used to quantify differential time-course trends between treatment conditions. A model with nested (replicate within hairpin) random effects structure was fit for each gene. A random-slope replicate-level random effect and a joint random intercept and slope hairpin-level random effect were specified. The fixed-effect portion of the model consisted of three parameters: the common initial measurement (β_0), the proliferation trend in untreated HCC827 (β_1), and the trend difference associated with Erlotinib treatment (β_E). The *t* statistic estimated for β_E was used to determine significance P-values using a *t* test, with degrees of freedom calculated using the "between-within"

rule[47]. P-values were subjected to false discovery rate (FDR) correction using the approach of Benjamini and Hochberg[48].

At the gene level, the magnitudes of β_1 and β_E are correlated, with larger decreases in proliferation in untreated cells (β_1) associated with larger magnitude differences between conditions (β_E). In other words, genes that are more essential in general tend to be associated with larger differences between conditions. An alternative measure of synthetic lethality considers the magnitude of the difference (β_E) relative to the magnitude of the baseline trend (β_1), thus estimating relative dependence of cell proliferation on a specified gene. We thus use an alternative measure of effect size to rank significant predictions, called the *Relative Dropout Rate*, defined as

$$\boldsymbol{sign}(\beta_E)\frac{\max(|\beta_1|,|\beta_1+\beta_E|)}{\min(|\beta_1|,|\beta_1+\beta_E|)+|median(\beta_1)|}$$

The median value of the genome-wide distribution of β_1, which is reliably modestly negative, is added to the denominator to avoid unusually large ratios.

The computation of mixed model variance parameter estimates by maximum likelihood may be problematic when the number of random effect groups is small, for example when three to five hairpins target a gene. In such cases estimates of variance parameters are frequently zero, and estimates of covariance matrices are often singular. Such estimates may artificially inflate significance assigned to model predictions. Boundary avoiding Bayesian priors can mitigate this issue by imposing a weakly informative prior on mixed model variance component estimates[49]. A Wishart prior is applied to the hairpin-level random intercept and slope covariance matrix, and a gamma prior is used for the replicate-level random slope variance, with each distribution using the default specified parameters[49]. Models were fitted using the R blme package.

Replicate measurements obtained from pooled shRNA screens are heteroscedastic, with replicate variance increasing both as mean measurement intensity decreases, and as measurement time-point (number of cell line doublings) increases. However, the small number of replicates makes reliable estimation of replicate variance difficult. Similarly to Anders and Huber[50], we assume a pooled variance estimate, with measurements taken at the same time-point, and with similar mean intensity, assumed to have similar variance. This smoothed variance estimate is estimated using local regression, and used to assign an inverse-variance (or dispersion) weight to each measurement modeled in the regression.

A detailed description of the method, which we term *siMEM*, and accompanying R software package, will be made available (unpublished data; Sayad A., Marcotte R., Neel B.G., and Moffat J.).

Methods references

41. Yang, X. et al. A public genome-scale lentiviral expression library of human ORFs. *Nat Methods* **8**, 659-661 (2011).
42. Lemercier, C. et al. mHDA1/HDAC5 histone deacetylase interacts with and represses MEF2A transcriptional activity. *J Biol Chem* **275**, 15594-15599 (2000).
43. Kurat, C.F. et al. Restriction of histone gene transcription to S phase by phosphorylation of a chromatin boundary protein. *Genes Dev* **25**, 2489-2501 (2011).
44. Brown, K.R. & Jurisica, I. Unequal evolutionary conservation of human protein interactions in interologous networks. *Genome Biol* **8**, R95 (2007).
45. Zhu, C.Q. et al. Understanding prognostic gene expression signatures in lung cancer. *Clin Lung Cancer* **10**, 331-340 (2009).
46. Marcotte, R. et al. Essential gene profiles in breast, pancreatic, and ovarian cancer cells. *Cancer Discov* **2**, 172-189 (2012).
47. Pinheiro, J.C. & Bates, D.M. Mixed-effects models in S and S-PLUS Springer. *New York* (2000).
48. Benjamini, Y. & Hochberg, Y. Controlling the false discovery rate: a practical and powerful approach to multiple testing. *Journal of the Royal Statistical Society. Series B (Methodological)*, 289-300 (1995).
49. Chung, Y., Rabe-Hesketh, S., Dorie, V., Gelman, A. & Liu, J. A nondegenerate penalized likelihood estimator for variance parameters in multilevel models. *Psychometrika* **78**, 685-709 (2013).
50. Anders, S. & Huber, W. Differential expression analysis for sequence count data. *Genome Biol* **11**, R106 (2010).

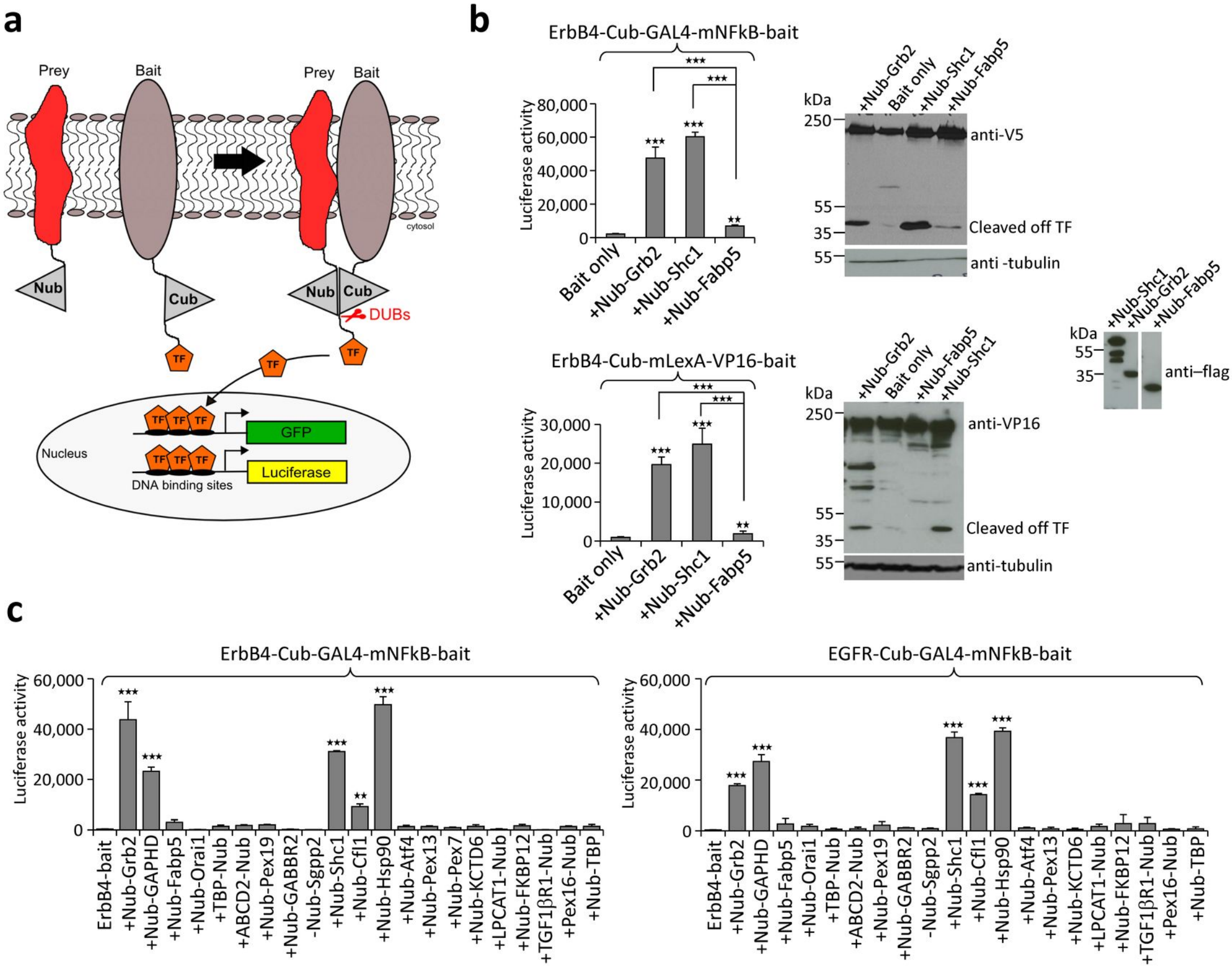
a
Prey
Bait
Prey
Bait
cytosol
Nub
Cub
Nub
Cub
DUBs
TF
TF
TF
Nucleus
GFP
Luciferase
DNA binding sites
b
ErbB4-Cub-GAL4-mNFkB-bait
Luciferase activity
80,000
60,000
40,000
20,000
0
Bait only
+Nub-Grb2
+Nub-Shc1
+Nub-Fabp5
kDa
250
55
35
55
anti-V5
Cleaved off TF
anti -tubulin
ErbB4-Cub-mLexA-VP16-bait
30,000
20,000
10,000
anti-VP16
anti-tubulin
anti–flag
c
ErbB4-Cub-GAL4-mNFkB-bait
EGFR-Cub-GAL4-mNFkB-bait
60,000
40,000
20,000
ErbB4-bait
+Nub-Grb2
+Nub-GAPHD
+Nub-Fabp5
+Nub-Orai1
+TBP-Nub
+ABCD2-Nub
+Nub-Pex19
+Nub-GABBR2
-Nub-Sgpp2
+Nub-Shc1
+Nub-Cfl1
+Nub-Hsp90
+Nub-Atf4
+Nub-Pex13
+Nub-Pex7
+Nub-KCTD6
+LPCAT1-Nub
+Nub-FKBP12
+TGF1βR1-Nub
+Pex16-Nub
+Nub-TBP

Figure 1

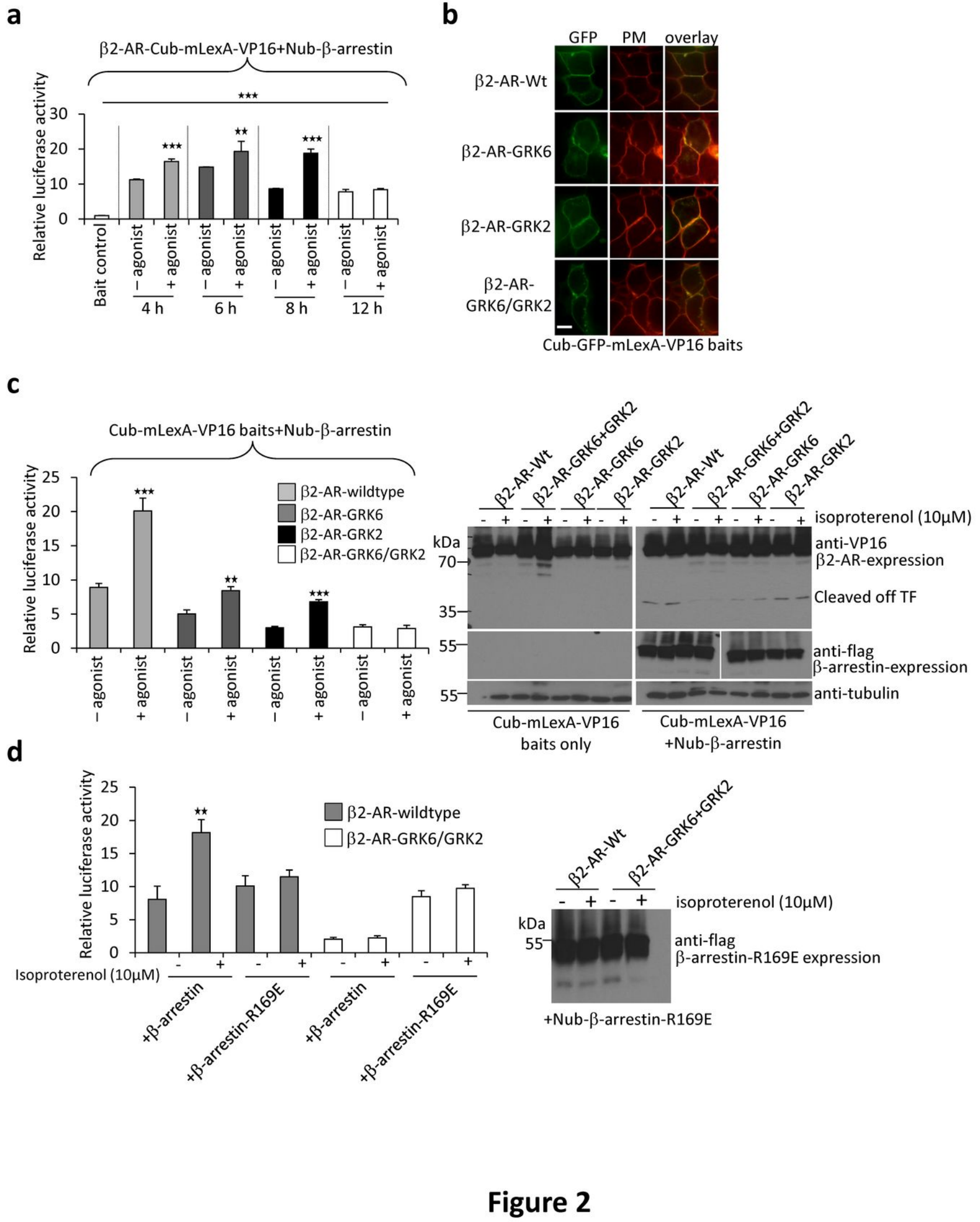
a
β2-AR-Cub-mLexA-VP16+Nub-β-arrestin
Relative luciferase activity
Bait control
– agonist
+ agonist
4 h
6 h
8 h
12 h
b
GFP
PM
overlay
β2-AR-Wt
β2-AR-GRK6
β2-AR-GRK2
β2-AR-GRK6/GRK2
Cub-GFP-mLexA-VP16 baits
c
Cub-mLexA-VP16 baits+Nub-β-arrestin
β2-AR-wildtype
β2-AR-GRK6
β2-AR-GRK2
β2-AR-GRK6/GRK2
isoproterenol (10μM)
kDa
anti-VP16
β2-AR-expression
Cleaved off TF
anti-flag
β-arrestin-expression
anti-tubulin
Cub-mLexA-VP16
baits only
Cub-mLexA-VP16
+Nub-β-arrestin
d
Isoproterenol (10μM)
+β-arrestin
+β-arrestin-R169E
anti-flag
β-arrestin-R169E expression
+Nub-β-arrestin-R169E

Figure 2

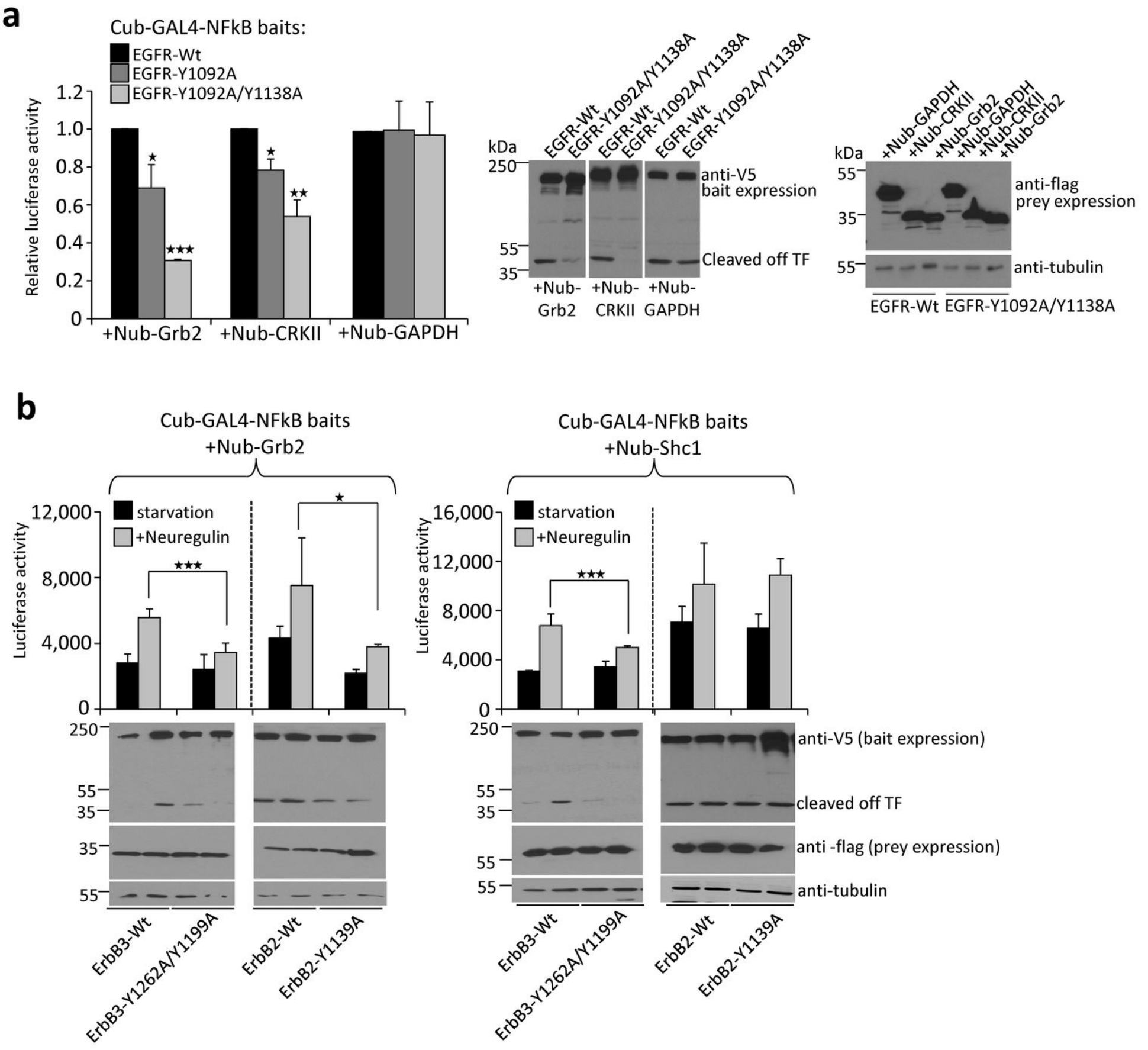
a
Cub-GAL4-NFkB baits:
EGFR-Wt
EGFR-Y1092A
EGFR-Y1092A/Y1138A
Relative luciferase activity
1.2
1.0
0.8
0.6
0.4
0.2
0
+Nub-Grb2
+Nub-CRKII
+Nub-GAPDH
kDa
250
55
35
anti-V5
bait expression
Cleaved off TF
+Nub-
Grb2
+Nub-
CRKII
+Nub-
GAPDH
anti-flag
prey expression
anti-tubulin
EGFR-Wt
EGFR-Y1092A/Y1138A
b
Cub-GAL4-NFkB baits
+Nub-Grb2
Cub-GAL4-NFkB baits
+Nub-Shc1
starvation
+Neuregulin
Luciferase activity
12,000
8,000
4,000
0
16,000
anti-V5 (bait expression)
cleaved off TF
anti -flag (prey expression)
anti-tubulin
ErbB3-Wt
ErbB3-Y1262A/Y1199A
ErbB2-Wt
ErbB2-Y1139A

Figure 3

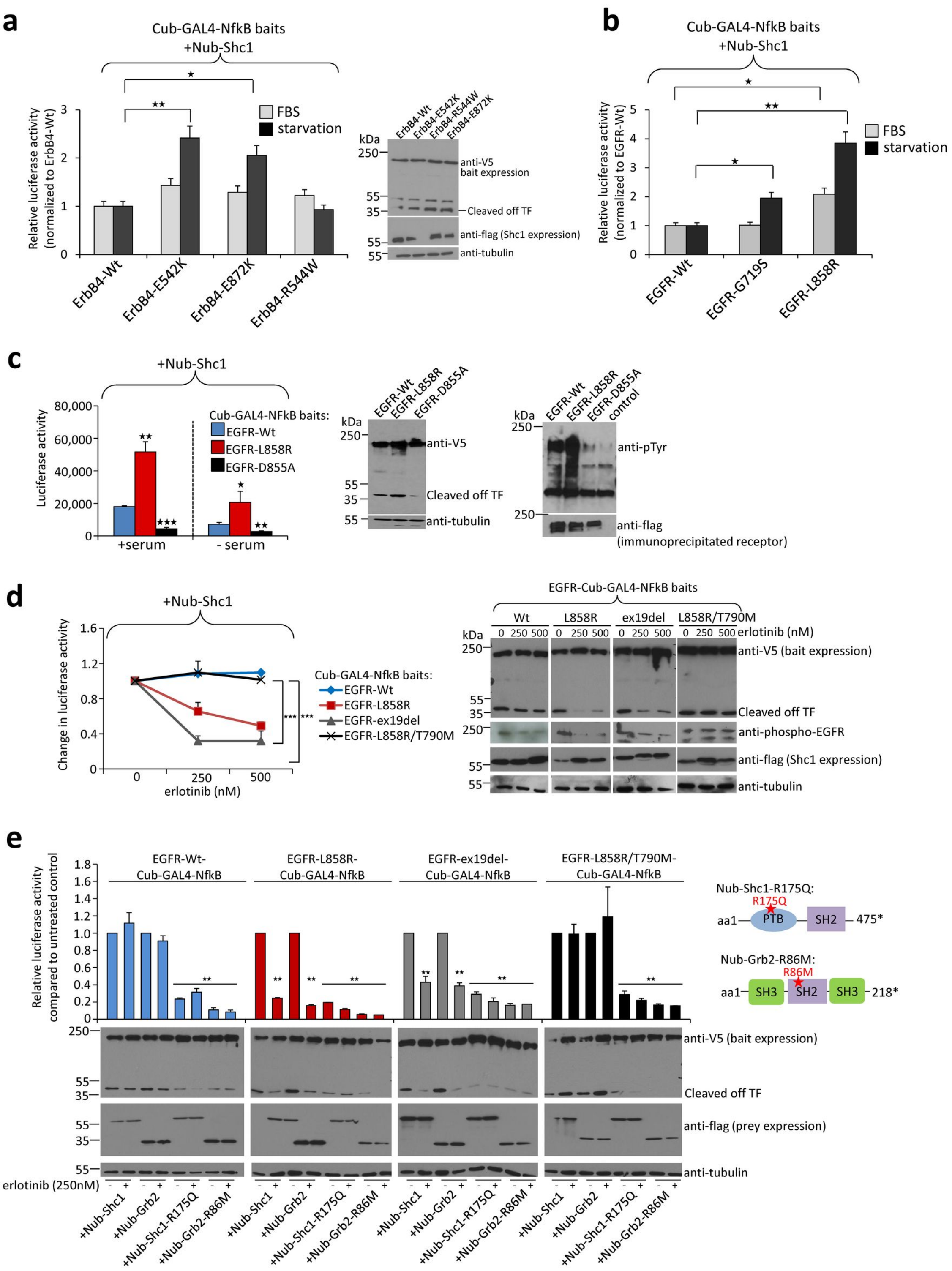
a
Cub-GAL4-NfkB baits
+Nub-Shc1
Relative luciferase activity (normalized to ErbB4-Wt)
FBS
starvation
ErbB4-Wt
ErbB4-E542K
ErbB4-E872K
ErbB4-R544W
kDa
250
55
35
anti-V5 bait expression
Cleaved off TF
anti-flag (Shc1 expression)
anti-tubulin
b
Cub-GAL4-NfkB baits
+Nub-Shc1
Relative luciferase activity (normalized to EGFR-Wt)
FBS
starvation
EGFR-Wt
EGFR-G719S
EGFR-L858R
c
+Nub-Shc1
Luciferase activity
Cub-GAL4-NFkB baits:
EGFR-Wt
EGFR-L858R
EGFR-D855A
+serum
- serum
kDa
anti-V5
Cleaved off TF
anti-tubulin
control
anti-pTyr
anti-flag
(immunoprecipitated receptor)
d
+Nub-Shc1
Change in luciferase activity
erlotinib (nM)
Cub-GAL4-NfkB baits:
EGFR-Wt
EGFR-L858R
EGFR-ex19del
EGFR-L858R/T790M
EGFR-Cub-GAL4-NFkB baits
Wt
L858R
ex19del
L858R/T790M
anti-V5 (bait expression)
Cleaved off TF
anti-phospho-EGFR
anti-flag (Shc1 expression)
anti-tubulin
e
Relative luciferase activity compared to untreated control
EGFR-Wt-Cub-GAL4-NfkB
EGFR-L858R-Cub-GAL4-NfkB
EGFR-ex19del-Cub-GAL4-NfkB
EGFR-L858R/T790M-Cub-GAL4-NfkB
Nub-Shc1-R175Q:
R175Q
aa1
PTB
SH2
475*
Nub-Grb2-R86M:
R86M
SH3
218*
anti-V5 (bait expression)
Cleaved off TF
anti-flag (prey expression)
erlotinib (250nM)
+Nub-Shc1
+Nub-Grb2
+Nub-Shc1-R175Q
+Nub-Grb2-R86M

Figure 4

a

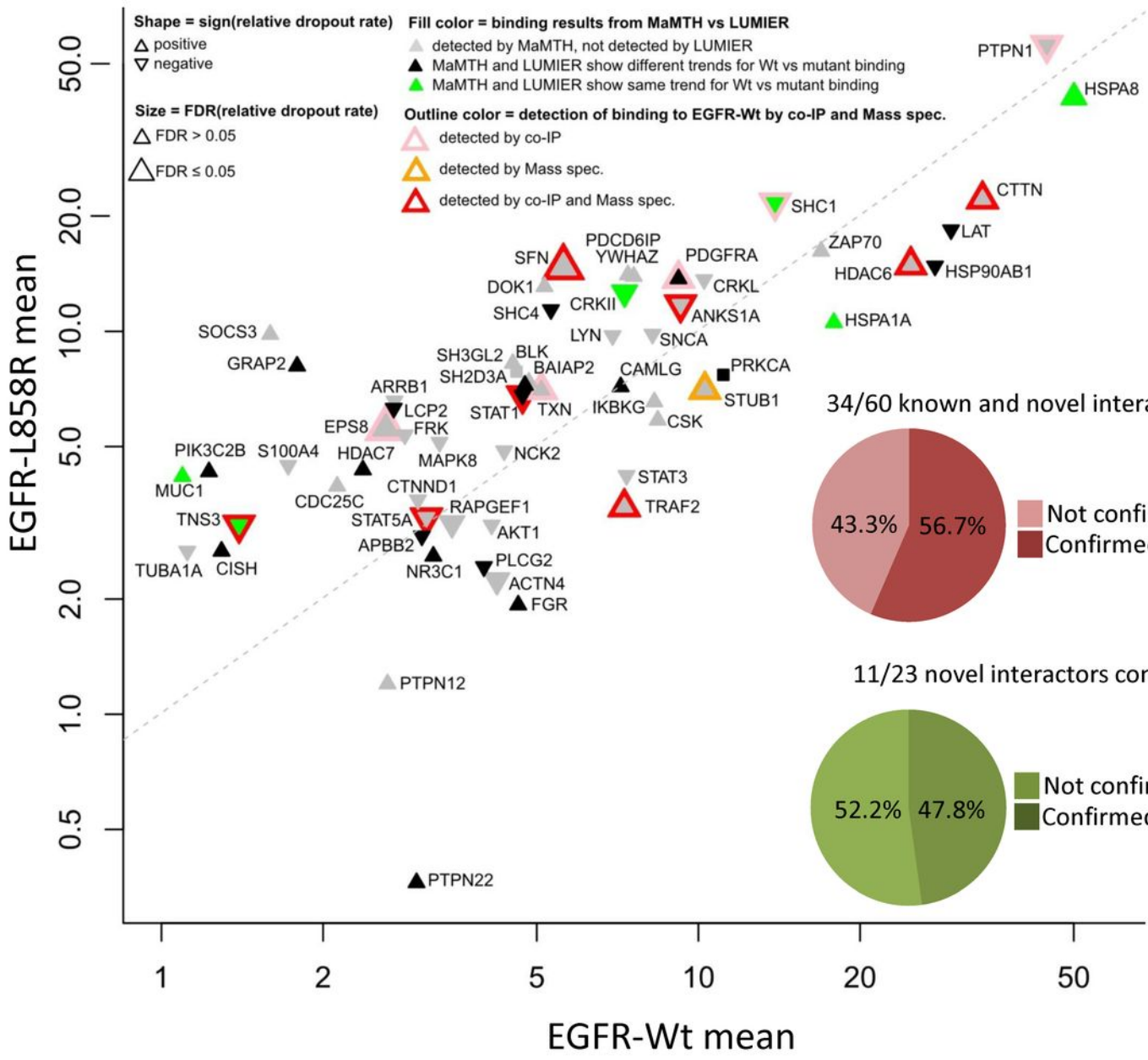

23 novel EGFR-interactors:

ACTN4
AKT1
ARRB1
BAIAP2
CDC25C
CTTN
DOK1
FGR
FRK
GRAP2
HDAC7
IKBKG
LAT
LCP2
MAPK8
NR3C1
PDGFRA
PTPN22
RAPGEF1
SHC4
SNCA
TNS3
S100A4

b

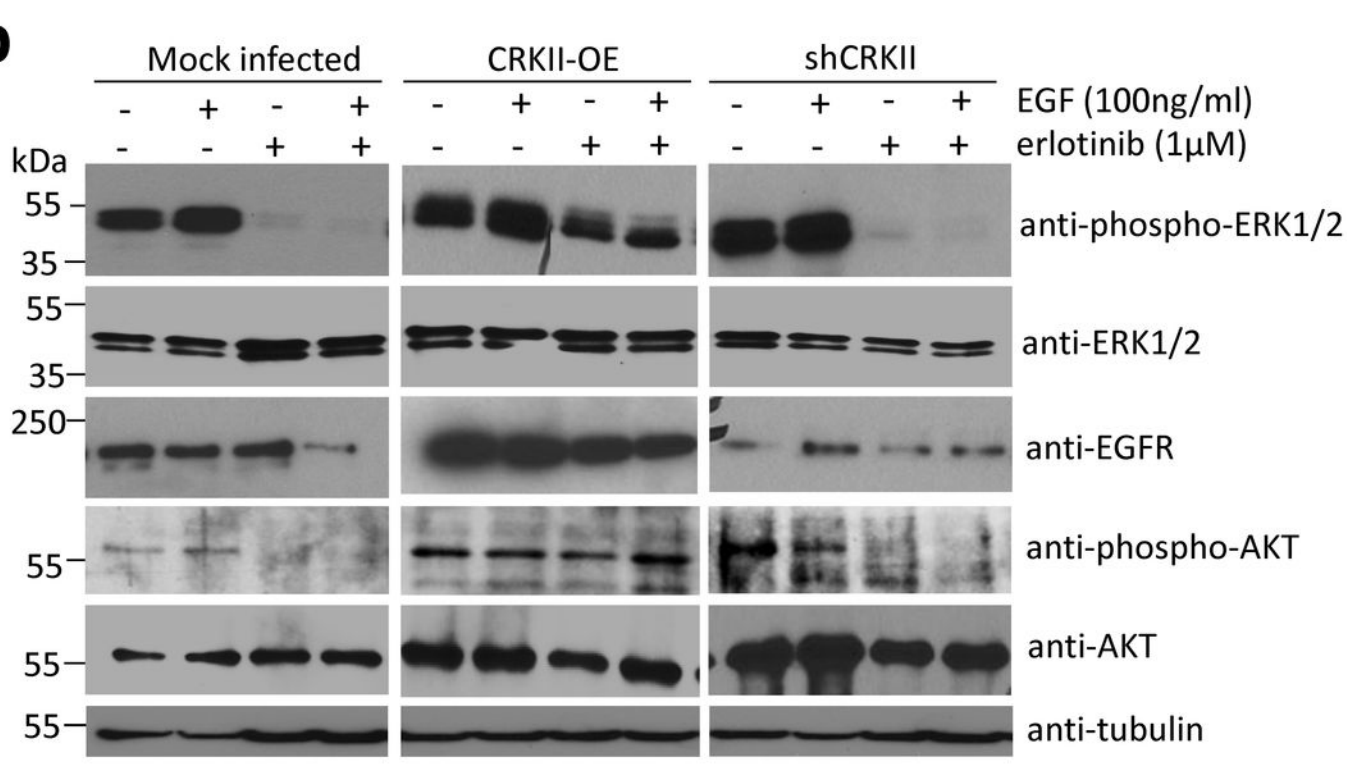

c

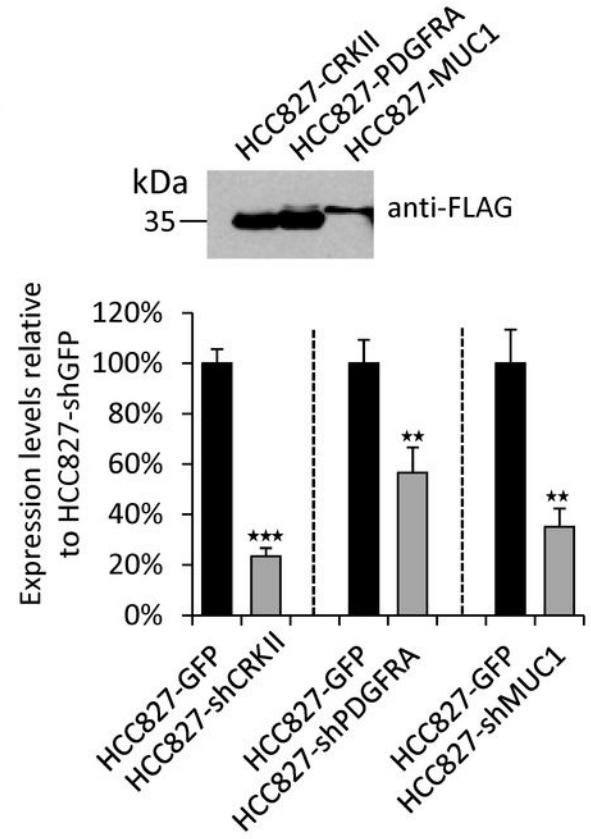

d

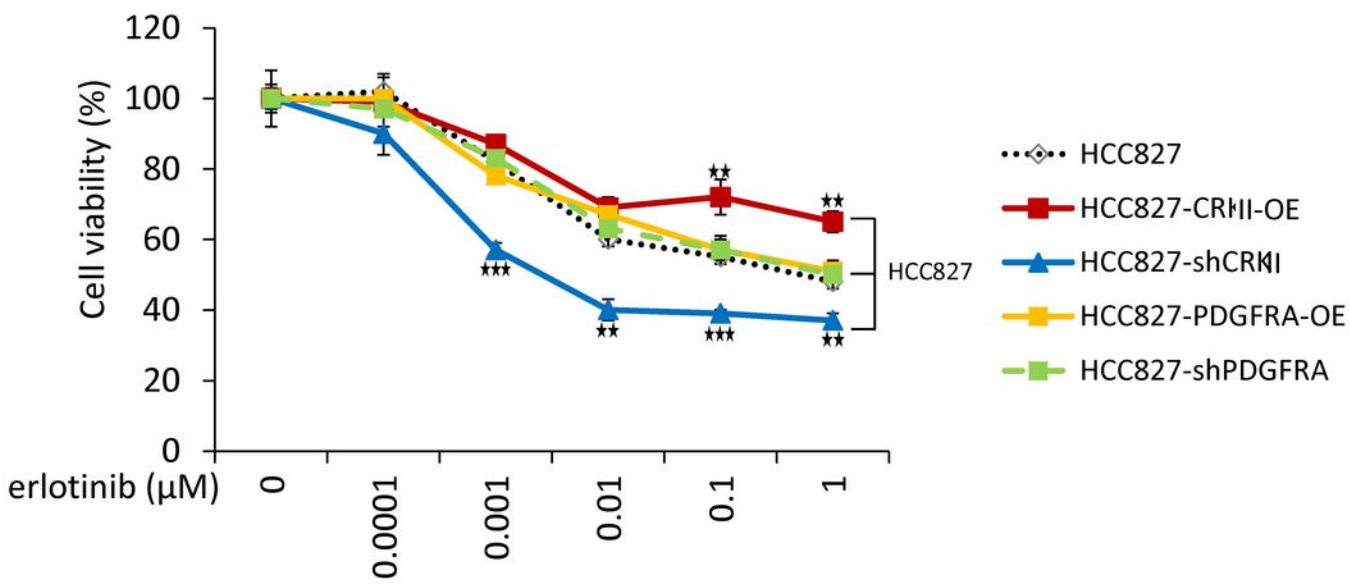

Figure 5